Available online at www.sciencedirect.com

ScienceDirect

Ciência & Tecnologia dos MATERIAIS

http://ees.elsevier.com/ctmat

Ciência & Tecnologia dos Materiais 28 (2016) 117–123

Special Issue on New Challenges in Energy Materials

Electrical and electrochemical properties of titanium dioxide /graphene nano platelets cathode for magnesium battery applications

M.H. Makled[a], Y.M. Arabi[a], E. Sheha[a,*], S. Arfa[a,d], I.S. Yahia[b,c], F. Salman[a]

[a]*Physics Department, Faculty of Science, Benha University, Benha, Egypt*
[b]*Semiconductor Labs., Faculty of Education, Ain Shams University, Roxy, Cairo, Egypt*
[c]*Physics Department, Faculty of Science, King Khalid University, Abha, Kingdom of Saudi Arabia*
[d]*Physics Department, Faculty of Science, Tabuk University, 71421, KSA*

Abstract

TiO_2/graphene nano platelets (GNP) nanocomposite cathodes have been synthesized through a simple ball mill process. TiO_2 anatase nanoparticles, around 16 nm in size, were encapsulated in the 2D graphene matrix. The synthesized samples are characterized using x-ray diffraction (XRD), DSC, impedance spectroscopy, and scanning electron microscope (SEM). The graphene nano platelets act not only to reduce the charge transfer resistance but can help to absorb deformation caused by divalent insertion. The electrochemical behavior of Mg metal was tested in dimethyl sulfoxide solution containing magnesium perchlorate salt. The obvious redox peaks on the cyclic voltammetric curves confirm Mg^{2+} inserts/extracts into/from TiO_2 through our simple electrolyte solution.

Keywords: Graphene; TiO_2; cathode; magnesium battery.

1. Introduction

Recently, a great attention has been focused on the high capacity, low cost and environment-friendly nature of the energy storage devices such as batteries [1]. Whereas, one of the main challenges that current rechargeable battery technologies face, is their ability to maintain energy and power densities sufficient to meet world energy demand. Lithium (Li) batteries are commonly used as a power source for large-scale energy storage applications and electronic devices because of their high energy density, high specific power, long cycling life time and safety [2]. However, lithium batteries cannot meet large volume applications like electric vehicle and electricity grid [3]. Now, magnesium has been foregrounded an alternative to lithium, due to its high theoretical specific charge capacity (2,205 A h/kg) and energy density (3.8 A h/cm^3), making it an excellent candidate as a metal battery anode [4]. In addition, Mg is easy handling, low cost comparing to Li (~$ 2700/ton for Mg compared to ~ $64,000/ton for Li) and abundant in the earth's crust (~13.9% Mg compared to ~0.0007% of Li) [5]. But, from other point of view, incompatible electrolyte with Mg anode and the sluggish kinetic of Mg^{2+} insertion/extraction hindered the development of Mg batteries [3, 6, 7]. So, the key challenges revolve around how to establish an electrolyte not to form a passivation layer on Mg metal during charge-discharge process, and develop a novel cathode that accept easy Mg^{2+} insertion/extraction. Recently, one of the promising cathode materials is nanostructured TiO_2 anatase compound which has great interest due to the low cost, and long-stability [8,9]. In spite of its advantageous

* Corresponding author.
E-mail address: islam.shihah@fsc.bu.edu.eg (E. Sheha)

http://dx.doi.org/10.1016/j.ctmat.2017.02.002

properties, TiO_2 suffers from low electrical conductivity, poor rate capability and poor cycling performance [10].

Graphene is an allotrope of carbon with sp^2 bond, where the carbon atoms are densely packed in a honeycomb crystal lattice [11]. These intrinsic characteristics can tune the electrical and mechanical properties of composite materials. Graphene sheets can be used due to its extraordinary electronic, thermal, and mechanical properties [2,12].

Recently, promising rechargeable magnesium battery based on Mg anode and a cheap and non-toxic commercial TiO_2 cathode was reported [13]. The electrolyte of the mentioned battery was synthesized from 0.5 mol L^{-1} $Mg(BH_4)_2/LiBH_4$/tetraglyme (TG) ($[LiBH_4]$ = 1.5 mol L^{-1}). The cell showed high specific capacity, excellent cycling stability, and rate capability. But, the used electrolyte is too costly and complicated. Furthermore, much work is needed to tune inter-layer spacing of TiO_2 so we can ease Mg^{2+} insertion/extraction.

Based on the above considerations, in this article, our strategy aims to synthesize a new simple electrolyte based on magnesium perchlorate salt dissolved in dimethyl sulfoxide more compatible with Mg anode than the previous research. In addition, we aim to tune inter-layer spacing of TiO_2 through doping with GNP and evaluate the effect of graphene on the physical and electrochemical properties of TiO_2. The composites will be characterized by means of X-ray diffraction (XRD), DSC, impedance spectroscopy, scanning electron microscopy (SEM) and cyclic voltammetry.

2. Experimental

To form the cathode pellet, TiO_2 anatase nanoparticles (QualiKems Chemical India) of purity 99 % were mixed with graphene nano platelet (XG-science) with purity 99.5% and 0.1 PVA as a binder in a ball mill at 400 rpm for 4 hrs. The graphene nano platelets (GNP) were incorporated in TiO_2 according to the formula $(TiO_2)_{1-x}(GNP)_x$, x= 0, 0.05, 0.1, 0.2, 0.4. Slurry of 85 wt % of TiO_2/GNP composites, 6 wt. % conductive agent (carbon black, Super-P-Li, 100 % purity from Gelon) and 9 wt% polyvinylidene difluoride (PVDF) binder in N-methyl-2-pyrrolidinone was pasted uniformly onto a copper foil, and dried in at 100 °C for 2 h.

To form the electrolyte, 2.5 g PVA were dissolved in 100 ml dimethyl sulfoxide followed by addition of 2.5 g ethylene carbonate (all from Qualikems India with purity 99%) and 3 g magnesium perchlorate (99.5% Sigma Aldrich), 5 g tetraethylene glycol dimethyl ether (TEGDME) (Aldrich, 99.9%), 0.5 g hydroquinone to moderate the corrosion of electrodes (99.5% Sigma Aldrich), and 20 ml distilled water, respectively. Molecular structure of the electrolyte is illustrated in Fig. 1.

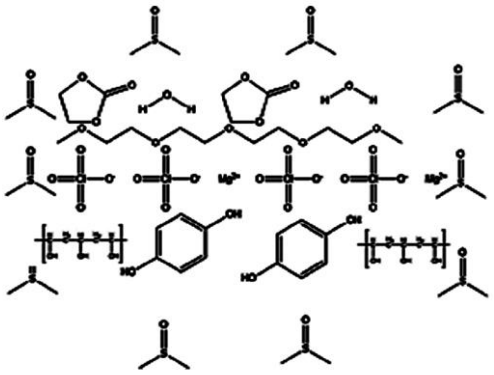

Fig. 1. Molecular structure visualization of $Mg(ClO_4)_2$ based electrolyte dissolved in dimethyl sulfoxide.

X-ray diffraction (XRD) patterns of the films were taken using a Rigaku diffractometer type RINT-Ultima IV/S. The diffraction system is based with Cu tube anode with voltage 40 kV and current 40 mA.

Thermo-gravimetric analyses (TGA) and Differential scanning calorimetry (DSC) of the prepared films were carried out using a Shimadzu–50 thermal analyzer from room temperature to 800 °C with a heating rate of 10 °C/min in a nitrogen atmosphere. For measuring dc conductivity, the current–voltage characteristics (*I–V*) of the $(TiO_2)_{1-x}(GNP)_x$ composites were recorded using a 2400 computer controlled Keithley electrometer. Samples of diameter 1.3 cm were sandwiched between the two similar stainless steel electrodes of a spring-loaded sample holder. The whole assembly was placed in a furnace monitored by a temperature controller. The rate of heating was adjusted to be 2 °C min^{-1}. Impedance measurements were performed on a Gwinstek LCR-811OG in the frequency ranging from 20 Hz to 10 MHz at different temperatures.

Cyclic voltammograms (CVs) were conducted in three-electrode cells using a CHI604E Electrochemical Workstation. TiO_2 and $(TiO_2)_{0.7}(GNP)_{0.3}$ nanocomposite were used as working electrode while magnesium ribbons were used as counter and reference electrodes (scan rate ~ 0.05 mV s^{-1}).

Table 1. Thermal decomposition energy E_a, particle size D and electrical activation energy E of $(TiO_2)_{1-X}$ (GNP)x composites.

GNP wt.%	E_a (J/mol)	D (nm)	E (eV)
0	93.66	16.3	0.603
5	86.02	15.3	0.138
10	68.43	34.7	-
20	61.16	34.7	-
30	56.38	33.1	-
40	68.81	36.2	-

3. Results and discussion

3.1. XRD analysis

Fig. 2 shows the XRD diffraction pattern of $(TiO_2)_{1-x}$ $(GNP)_x$ composite. In the case of free TiO_2, all the diffraction peaks can be perfectly indexed to the typical anatase with tetragonal structure of TiO_2 [2,14,15]. Diffraction peaks (002) at 2θ=26 ºC were observed in TiO_2 doped graphene, which could be associated with the ordering of graphene in TiO_2 – graphene network. The ordered peak becomes sharper with increasing GNP content which is a strong evidence of uniform distribution of graphene nano platelets (GNP) in TiO_2 matrix [16].

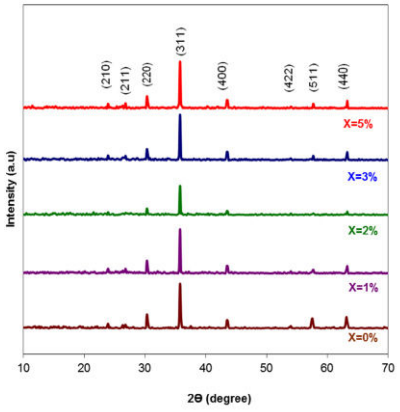

Fig. 2. X-ray diffraction pattern of $(TiO_2)_{1-X}$ $(GNP)_X$ composite.

The particle size D values of $(TiO_2)_{1-x}$ $(GNP)_x$ composite are listed in Table 1 and were calculated using the Scherrer's equation [17]:

$$D = \frac{\kappa\lambda}{B\cos\theta} \quad (1)$$

where λ is the wavelength of X-ray (0.154nm), K is a constant ~ 0.9, B is the full width at half maximum and θ is Bragg' s angle of anatase (101) plane.

3.2. TGA analysis

Fig. 3a) shows the TGA spectra of $(TiO_2)_{1-x}$ $(GNP)_x$ composites. No weight loss of TiO_2 nanoparticles was observed during this process (x=0) [18]. On the other hand, the water vaporization for the composites was difficult to record.

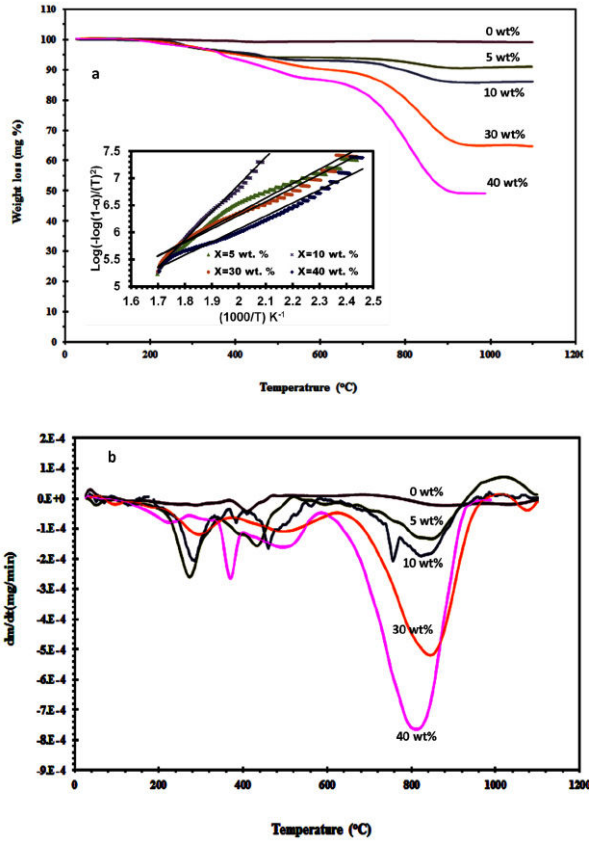

Fig. 3. (a) TGA analysis and (b) DTG analysis of $(TiO_2)_{1-x}$ $(GNP)_x$ composite.

A first weight loss from 270 to 370 ºC can be attributed to the elimination of OH groups and chain-scission reactions [19, 20]. The second weight loss from 433 to 493 ºC is related to the primary decomposition of grapheme. Normally, graphene decomposes at relatively low temperature about 650 ºC [21]. The thermal behavior of $(TiO_2)_{1-x}$ $(GNP)_x$ composites are further probed using the derivative thermogram (DTG) curves (Fig. 3b). The two peaks observed at 270 °C and 800 °C, may be attributed to

the thermal decomposition of PVA (binder) and GNP, respectively [19,20,22].

The dependence of the activation energies for the thermal decomposition of the present samples on the residual mass can be calculated using the first order integral equation of Coates and Redfern [23]**:**

$$Log[\frac{-Log(1-\alpha)}{T^2}] = Log\frac{R}{\Delta E}[1-\frac{2RT}{E}] - \frac{E}{2.304RT} \quad (2)$$

where, T is the absolute temperature in Kelvin, E is the activation energy in J/mol, *R* is the universal gas constant (8.13 J/mol K^{-1}) and the fraction of conversion, α, for a weight loss, is given by:

$$\alpha = \frac{w_i - w_t}{w_i - w_f} \quad (3)$$

where w_t, w_i and w_f are the actual, initial and final weight of the samples, respectively. By plotting the dependence of *-Log [-Log (1- α)/T^2]* versus *1000/T* for each sample, we obtain straight lines, (Fig. 3a (inset)). Then, the apparent decomposition energies, *E,* are calculated from the slopes of these lines using the expression:

$$E = 2.303R \times slope \quad (4)$$

Values are listed in Table1. From this table, it clears that the values of the activation energy decreased with increasing graphene content. This reflects the role of GNP to disrupt the chemical nature of TiO_2, which may be advantageous for their potential applications in electrochemical devices.

SEM micrograph of TiO_2 and $(TiO_2)_{1-x}$ $(GNP)_x$ nanocomposites are shown in Fig. 4. In the case of free graphene, Fig. 4a), TiO_2 nanoparticles aggregate into large particles, which could be attributed to poor rate performance as an anode material due to the long diffusion path for ions transport during ions insertion/extraction process [2]. By incorporating GNP in TiO_2 matrix, the later was found to be uniformly distributed in GNP and well distributed on the 2D graphene nanoplatelets, as shown in Figs. 4 b-c). It was also noticed that graphene nanoplatelets are crumpled to a curly and wavy shape. This unique structure is expected to facilitate the transports of Mg^{2+} ions, leading to high specific capacity and high rate capability [16].

3.3. Conductivity Analysis

Fig. 5a) shows the current–voltage (I&V) characteristics of the $(TiO_2)_{1-x}$ (GNP)x composites for different graphene concentrations. The current increases linearly with increasing voltage, obeying Ohm´s law. The values of the resistivity were extracted from the figure according to equation (5),

$$\sigma_{dc} = \frac{1}{R} \times \frac{L}{A} \quad (5)$$

where L is the thickness of the sample and A is the surface area of the sample. On the other hand, a significant change of the composites resistivity was recorded with increasing GNP concentration.

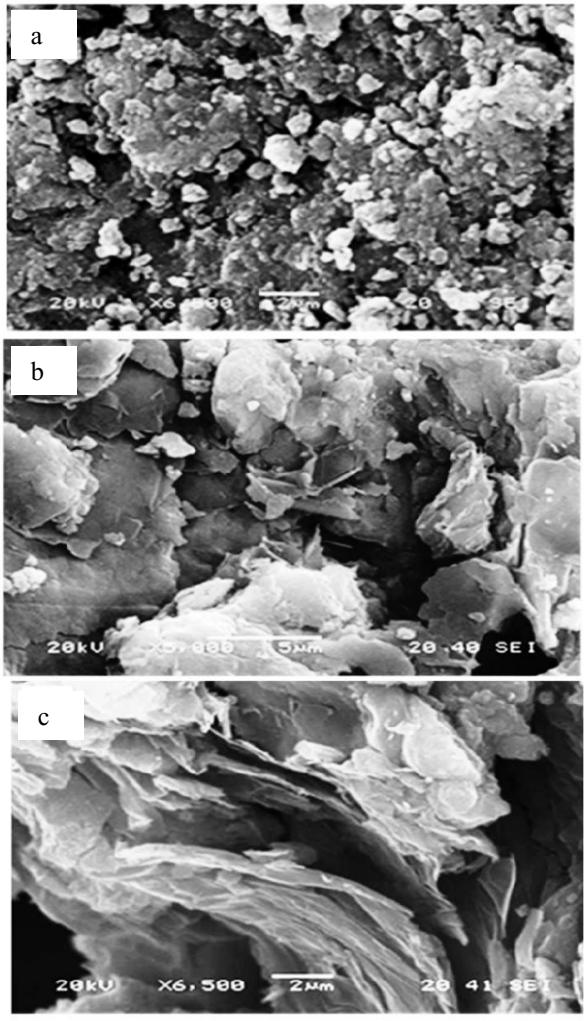

Fig. 4. SEM analysis of $(TiO_2)_{1-x}$ $(GNP)_x$ composite for (a) TiO_2, (b) x= 20 and (c) x=40 wt % GNP.

The effect of graphene content on the dc conductivity σ_{dc} of $(TiO_2)_{1-x}$ (GNP)x is shown in Fig. 5b). The dc conductivity of the composites exhibits insulator behavior for pure TiO_2 recording ~10 $x10^{-10}$S/cm, whereas a semiconductor behavior was recorded for low graphene content up to 5 vol. %.

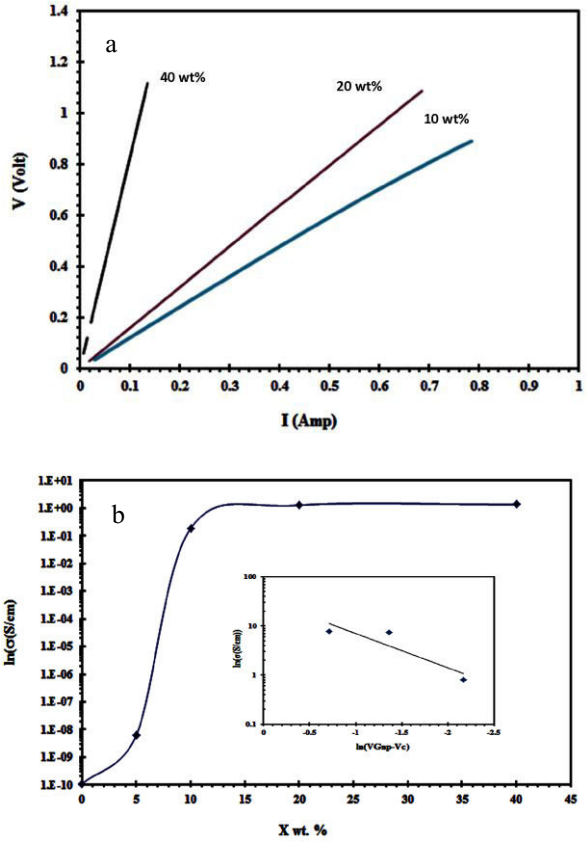

Fig. 5. (a) I–V curves and (b) DC conductivity concentrations dependence of $(TiO_2)_{1-x}$ $(GNP)_x$ composite.

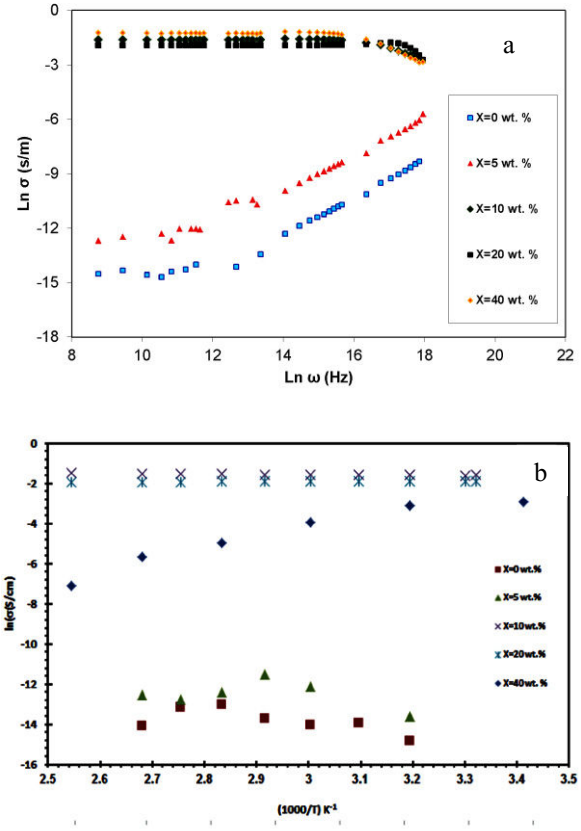

Fig. 6. (a) Variation of conductivity with frequency and (b) Variation of conductivity with temperature for $(TiO_2)_{1-x}$ $(GNP)_x$ composites.

The electrical conductivity increased sharply as the content of graphene was close to percolation threshold up to 5 vol. %. Above the percolation threshold, unnoticeable increasing in σ_{dc} was recorded due to the formation of filler network and the composites reaches metallic electrical behaviors.

The dependence of the electrical conductivity on the GNP volume fraction V_{GNP} can be described according to the percolation theory, obeying the following power relation at $V_{GNP} > V_C$ [24],

$$\sigma_{dc} = \sigma_c \, (V_{GNP} - V_C)^t \qquad (6)$$

where σ_c is the conductivity of the conducting component, V_C is the critical volume fraction or percolation threshold, and the exponent t reflects the dimensionality of the system and has been calculated to be 1.3 or 2.0 corresponding to two and three dimensions, respectively [25]. Fig. 5b) (inset) shows a fitting of percolation equation for $(TiO_2)_{1-x}(GNP)_x$ composites. The exponent t was found to be about 1.61.

This result confirms that the GNP nanoparticles are not located on the surface of the host material matrix particles, but that they are coordinated in the TiO_2 crystal structure and the formation of graphene three dimensional networks could be enhanced. According to the obtained values of the exponent t, X-ray results and SEM investigation, one can conclude that, the charge will transport easily through the three dimensional network of graphene and that the tunneling of charge carrier between weakly connecting parts of the network will be predominant especially at high GNP content [24-26]. The higher values of exponent t could be related to the aspect ratio (r/*l*) of graphene nano platelets particles, where *r* is the particle thickness and *l* is the particle length. For nanotubes or nanosheets particles, the aspect ratio will be small leading to critical percolation and three dimensional network at low volume fraction [27, 28].

Fig. 6a) shows the dependence of conductivity on frequency, at room temperature, for the present composites at different GNP content. Before

percolation, the conductivity exhibits two distinct regions: low-frequency region and high-frequency region. At low frequencies, a plateau characterized by direct current conductivity (DC) is present, while at high frequencies, the conductivity increases gradually with increasing frequency. This behavior obeys the universal power law

$$\sigma = \sigma_{dc} + A\omega^{s} \quad (7)$$

where σ_{dc} is the dc conductivity, ω is the angular frequency, *A* is the pre-exponential factor and s is the conduction mechanism factor lies in the range 0<s <1 [29, 30].

The values of the exponent s were calculated from the fitting of the relation between $\ln\sigma_{ac}$ versus lnω. The *s* found values lie within the range of 0.6 < *s* <0.7, which predict the predominance of hopping conduction in $(TiO_2)_{1-x}$ (GNP)x composites before percolation [31]. On the other hand, for samples with high graphene content (10, 20 and 40 wt. %) the electrical conductivity is frequency independent, recording metallic behavior and predominance of tunneling conduction due to the formation of graphene network. The decay of conductivity at very high frequency is attributed to the high speed of the electric field and the charge carrier cannot follow it.

Fig. 6b) shows the temperature dependence of ac conductivity for $(TiO_2)_{1-x}$ (GNP)x composites at 1 K Hz. Form the figure, on can notice that, three distinct behaviors of the composites conductivity with temperature are recorded. At low GNP content, less than percolation threshold, the conductivity reflects semiconductor behaviors, while at moderate and high GNP content, the conductivity recorded semimetal and metallic behaviors respectively.

For the samples 0 and 5 wt. %, the conductivity of the materials follows Arrhenius behavior, i.e.

$$\sigma = \sigma_0 \exp\left[\frac{\pm E_a}{KT}\right] \quad (8)$$

where σ_0 is the pre-exponential factor, E_a is the activation energy, K is the Boltzmann constant, and T is the temperature in Kelvin [32]. The unchanged or the decreasing of σ with temperature at high GNP concentration, could be attributed to the breakdown of extended graphene and scattering of charge with increasing temperature [33].

The values of E_a are calculated from the fitting of the relation between $\ln\sigma_{ac}$ versus 1000/T and listed in Table 1 for the low GNP content samples. The values of activation energy decrease with increasing graphene content, which could be attributed to crosslink of the conductive paths by GNP through the whole composite.

3.4. Electrochemical studies

Cyclic voltammogram (CV) techniques were used to investigate the electrochemical behavior of the TiO_2 and $(TiO_2)_{0.7}(GNP)_{0.3}$ nanocomposite as the working electrodes for electrochemical magnesium storage. Ten cycles were conducted for each cell. Fig. 7 shows the cyclic voltammetry curve in three-electrode Mg cell, where TiO_2 and $(TiO_2)_{0.7}(GNP)_{0.3}$ composites are working electrodes and Mg ribbons are counter and reference electrodes, respectively.

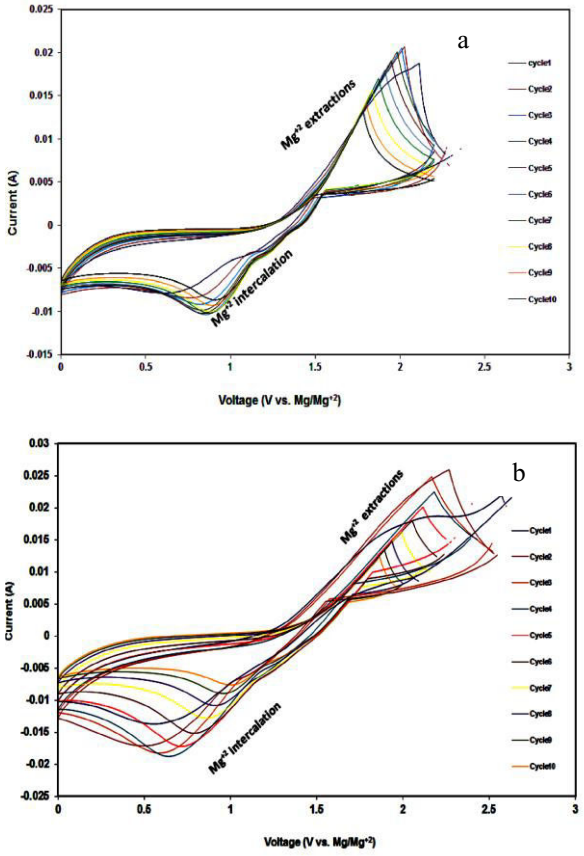

Fig. 7. CV curves of the as prepared working electrodes (a) TiO_2 (b) $(TiO_2)_{0.7}/(GNP)_{0.3}$.

The voltammograms show typical features of the electrochemical magnesium de-intercalation and intercalation reactions. Mg^{2+}de-intercalation and intercalation can be distinguished, corresponding to anodic/cathodic peaks at ~ 2 V (A) and 0.5 V (C), respectively. As the cycle number increase the anodic

peak shifted slightly to a more negative potential while the cathodic peaks partly moved to a more positive potential. Furthermore, the height of characteristic peaks decrease with repeated cycling. This can be attributed to undesirable reaction [31]:

$$Mg + H_2O \rightarrow MgO + H_2$$

formation of non-Mg^{2+} conducting molecules (*MgO*) at anode surface which can moderate kinetic of Mg^{2+}. Fig. 8 shows schematic representation of electrochemical Mg^{2+} insertion/extraction mechanism within Mg cell. The chemical reaction that probably takes place at the cathode is:

$$TiO_2 + xMg(II) + 2xe \Leftrightarrow Mg_xTiO_2$$

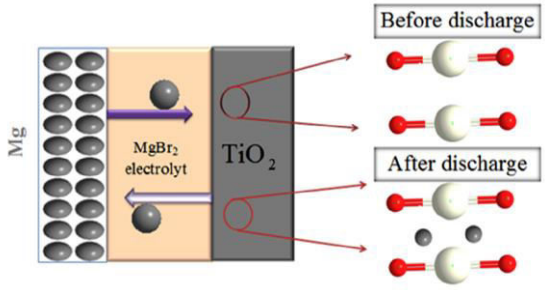

Fig. 8. Electrochemical mechanism of the TiO_2/GNP nanocomposite electrode within an Mg cell.

4. Conclusion

TiO_2/GNP composites were synthesized by a ball mill method. SEM and X-ray analyses confirmed that graphene is well distributed in TiO_2. It is evident that graphene helped to reduce the charge transfer resistance and can absorb deformation caused by divalent insertion in TiO_2. Obvious redox peaks on the cyclic voltammetric curves confirm Mg^{2+} inserts/extracts into/from TiO_2 through our simple electrolyte solution similar to that observed in conventional Grignard reagents.

References

[1] V. Palomares, P. Serras, I. Villaluenga, K.B. Hueso, J.C. Gonzalez and T. Rojo, Energy Environ. Sci. 5 (2012) 5884-5901.

[2] N. Sa, H. Wang, D.L. Proffit, A.L. Lipson, B. Key, M. Liu, Z. Feng, T.T. Fister, Y. Ren, C.-J. Sun, J.T. Vaughey, P.A. Fenter, K.A. Persson, A.K. Burrell, J. Power Sources 323 (2016) 44-50.

[3] I.-T. Kim, K. Yamabuki, M. Sumimoto, H. Tsutsumi, M. Morita, N. Yoshimoto, J. Power Sources 323 (2016) 51-56.

[4] F. Tuerxun, Y. Abulizi, Y. NuLi, S. Su, J. Yang, J. Wang, J. Power Sources, 276 (2015) 255-261.

[5] E. Sheha, M.M. Nasr, M.K. El-Manly, Mater. Sci. Techno. 31(2015) 1113-1121.

[6] E. Sheha, A. Bassyouni, Energy Environ. Focus 5 (2016) 1–6.

[7] G. Gershinsky, H.D. Yoo, Y. Gofer, D. Aurbach, J. Amer. Chem. Soc. 29 (2013) 10964–10972.

[8] L. Tan, C. Cao, H. Yang, B. W. Lei Li, Mater. Lett. 109 (2013) 195-198.

[9] W. J. Zhou, Y. H. Leng, D. M. Hou, H. D. Li, L. G. Li, G. Q. Li , H. Liu W. Chen, The Royal Soc. Chem. 6 (2014) 4698-4704.

[10] A.K. Rai, L.T. Anh, J. Gim, V. Mathew, J. Kang, B.J. Paul, J. Song, J. Kim, Electrochim. Acta 90 (2013) 112-118.

[11] Q. Xiang, J. Yu, M. Jaroniec, Chem. Soc. Rev. 41 (2012) 782-796.

[12] R.K. Layek, S. Samanta, D.P. Chatterjee, A.K. Nandi, Polymer 51 (2010) 5846-5856.

[13] S. Su, Z. Huang, Y.N. Li, F. Tuerxun, J. Yang, J. Wang, Chem. Commun. 51 (2015) 2641-2644.

[14] J. Wang, Y. Zhou, B. Xiong, Y. Zhao, X. Huang, Z. Shao, Electro. Acta 88 (2013) 847-857.

[15] K. Karthik, S. K. Pandian, N. V. Jaya, Appl. Surf. Sci. 256 (2010) 6829-6833.

[16] D. Cai, D. Li, S. Wang, X. Zhu, W. Yang, S. Zhang, H. Wang, J. Alloy Comp. 561 (2013) 54-58.

[17] W. Low, V. Boonamuayvitaya, J. Environ. Manag. 127 (2013) 142-149.

[18] H.C. Tao, L.Z. Fan, X. Yan, X. Qu, Electro. Acta 69 (2012) 328-333.

[19] M.B. Radoicic, Z.V. Šaponjic, M.T. Marinovic-Cincovic, S.P. Ahrenkiel, N.M. Bibic and J.M. Nedeljkovic, J. Serb. Chem. Soc. 77 (2012) 699-714.

[20] T.A. Kareem, A.A. Kaliani, Arabian J. Chem. 4 (2011) 325-331.

[21] Y.L. Min, G.Q. He, R.B. Li, W. Zhao, Y.C. Chen, Y.G. Zhang, Sep. Purif. Technol. 106 (2013) 97-104.

[22] M. Mehrali, S.T. Latibari, M. Mehrali, T.M.I. Mahlia, H.S.C. Metselaar, M.S. Naghavi, E. Sadeghinezhad, A.R. Akhiani, Appl. Therm. Eng. 61 (2013) 633-640.

[23] E.M. Abdelrazek, I.S. Elashmawi, and S. Labeeb; Physica B 405 (2010) 2021.

[24] Y. Fan, L. Wang, J. Li, J. Li, S. Sun, F. Chen, L. Chen, W. Jiang, Carbon 48 (2010) 1743-1749.

[25] H. Pang, T. Chen, G. Zhang, B. Zeng, Z. Li, Mater. Lett. 64 (2010) 2226-2229.

[26] S. Rul, F. Lefevre-Schlick, E. Capria, C. Laurent, A. Peigney, Acta Mater. 52 (2004) 1061-1067.

[27] M. Makled, H. Washiya, H. Tsuda, Appl. Polym. 113 (2009) 3294-3299.

[28] M. H. Makled, Appl. Polym. 126 (2012) 969-973

[29] M. Okutan, E. Basaran, H.I. Bakan, F.Yakuphanoglu, Physica B 364 (2005) 300-305.

[30] D. Wang, X. Zhang, J.W. Zha, J. Zhao, Z. Dang, G.H. Hu, Polym. 54 (2013) 1916-1922.

[31] M.H. Makled, E. Sheha, T.S. Shanap, M.K. El-Mansy, J. Advanced Research 4 (2013) 531-538.

[32] E. Thirumal, D. Prabhu, K. Chattopadhyay, V. Ravichandran, J. Alloy. Compd. 502 (2010) 169-175.

[33] M.H. Ali, A. Abo-Hashem, J. Mater. Process. Technol. 68 (1977) 163-167.